Title	First-principles prediction of low-energy structures for AlH3
Author(s)	Sun, Shoutian; Ke, Xuezhi; Chen, Changfeng; Tanaka, Isao
Citation	PHYSICAL REVIEW B (2009), 79(2)
Issue Date	2009-01
URL	http://hdl.handle.net/2433/84628
Right	© 2009 The American Physical Society
Type	Journal Article
Textversion	publisher

First-principles prediction of low-energy structures for AlH_3

Shoutian Sun,[1] Xuezhi Ke,[1,2,*] Changfeng Chen,[2,†] and Isao Tanaka[3,‡]
[1]*Department of Physics and Institute of Theoretical Physics, East China Normal University, Shanghai 200062, China*
[2]*Department of Physics and High Pressure Science and Engineering Center, University of Nevada, Las Vegas, Nevada 89154, USA*
[3]*Department of Materials Science and Engineering, Kyoto University, Sakyo, Kyoto 606-8501, Japan*
(Received 30 July 2008; revised manuscript received 27 October 2008; published 9 January 2009)

We report density-functional calculations that predict ten different low-energy structures for aluminum hydride AlH_3 with space groups *Pnma*, *P*6/*mmm*, *I*4/*mcm*, *P*4/*mbm*, *P*4/*nmm*, $Pm\bar{3}m$, $P2_1/m$, $P2_1/c$, *Pbcm*, and *P*4/*n*. Phonon calculations within harmonic approximation reveal unstable modes in the *P*6/*mmm*, *I*4/*mcm*, *P*4/*mbm*, *P*4/*nmm*, $Pm\bar{3}m$, $P2_1/m$, and $P2_1/c$ structures, indicating that they are unstable at low temperatures. The calculations show that the thermodynamic stabilities for AlH_3 with space groups *Pnma*, *Pbcm*, and *P*4/*n* are overall close to the existing α- and γ-AlH_3. From x-ray powder-diffraction patterns, the simulated main-peak positions for AlH_3 (*P*4/*n*) are in good agreement with experimental δ-AlH_3. A full Rietveld analysis reveals that the fitting space groups $R\bar{3}c$, *Pbcm*, and *Pnma* to the experimental x-ray powder-diffraction pattern of α-AlH_3 gives almost the same satisfactory result.

DOI: 10.1103/PhysRevB.79.024104 PACS number(s): 71.15.Mb, 61.66.Fn, 65.40.−b

I. INTRODUCTION

Recently, aluminum hydride AlH_3 has received considerable attention both in theory[1–11] and experiment[12–22] since this material has important applications as a possible hydrogen storage medium, an energetic component in rocket propellants, and a reducing agent in alkali batteries.[23] For the purpose of hydrogen storage, this material could be an excellent candidate if it can be cheaply produced and appropriate catalysts can be found, since it has a total capacity of 10.1 wt % hydrogen, and hydrogen can be released upon heating to slightly over 373 K.[23] The decomposition of AlH_3 may take place in a single step,

$$AlH_3 \rightarrow Al + \frac{3}{2}H_2, \tag{1}$$

This material (α phase) is known to be thermodynamically unstable near ambient conditions, but it is kinetically stable without releasing much hydrogen for years. At least seven polymorphs of AlH_3 have been detected in experiments[24] but only four have been crystallographically determined, i.e., α (in Ref. 25), α' (in Ref. 12), β (in Ref. 17), and γ (in Refs. 18 and 19) phases. The crystal structures of the other polymorphs are still unknown and remain to be determined. We previously predicted two different crystal structures for AlH_3 using first-principles calculations, which have been confirmed by experiments (identified as α' phase in Ref. 12 and β phase in Ref. 17). In the present work, we extend our search for different AlH_3 phases with a particular focus on a wide variety of AB_3-type candidates. Our extensive search [combining *ab initio* molecular dynamics (MD)] has resulted in the identification of ten different low-energy structures for AlH_3. In Secs. II–IV, we first present the computational methods, followed by a systematic analysis of the structural features, dynamic stability, and thermodynamic functions of these different structures.

II. THEORETICAL METHODS

The first-principles calculations have been performed in the framework of the density-functional theory[26,27] using the generalized gradient approximation (GGA) (Ref. 28) as implemented in the VASP code.[29,30] The interaction between the ion and electron is described by the all-electron projector augmented wave (PAW) method.[31,32] The configurations Al $3s^2 3p^1$ and H $1s^1$ were treated as the valence electrons. Brillouin-zone integrations were performed on the grid of Monkhost-Pack procedure.[33] For each supercell, a dense *k*-point mesh (spacing of *k* point $<0.1/$Å) and a high plane-wave cutoff energy of 600 eV were used. The total-energy convergence within 0.5 meV/f.u. was achieved.

To check the mechanical stability and the thermodynamic functions for these different crystals, the harmonic phonons were calculated by a direct *ab initio* force-constant approach implemented by Parlinski *et al.*[34,35] In this method a specific atom is displaced to induce the forces on the surrounding atoms, which are calculated via the Hellmann-Feynman theorem (output from VASP code). The forces are collected to construct the force-constant matrices. Harmonic phonons were obtained from the diagonalization of the dynamical matrices. The supercell sizes for current phonon calculations are compiled in Table I. The internal energy ($E_{(T)}$) was evaluated from the integral of phonon density of state (DOS) as follows:

$$E_{(T)} = \frac{1}{2} r \int_0^\infty \hbar\omega g(\omega) \coth\left(\frac{\hbar\omega}{2k_B T}\right) d\omega, \tag{2}$$

where r is equal to $3N$ (N is the number of atoms in a unit cell), $g(\omega)$ is the phonon DOS, $\hbar$ is the Planck constant, k_B is the Boltzmann constant, and T is temperature. Similar integrals can be applied to calculate the zero-point (ZP) energy, entropy ($S_{(T)}$), and free energy ($F_{(T)}$).[36]

To study the decomposition reaction in Eq. (1), one needs to examine the Gibbs free energy for H_2 gas at elevated temperatures. At atmospheric pressure, the Gibbs free energy

TABLE I. Supercell size and Monkhorst-Pack k-point mesh for phonon calculations.

Structures	Lattice constants of supercells (Å; deg)	k-point mesh
α-AlH_3 ($R\bar{3}c$)	$a=b=c=9.43$; $\alpha=\beta=\gamma=56.84$	$3\times3\times3$
γ-AlH_3 ($Pnnm$)	$a=10.88$, $b=7.41$, $c=11.59$; $\alpha=\beta=\gamma=90$	$2\times3\times2$
Cubic AlH_3 ($Pm\bar{3}m$)	$a=b=c=10.25$	$2\times2\times2$
Orthorhombic AlH_3 ($P2_1/m$)	$a=13.12$, $b=6.58$, $c=6.54$; $\alpha=\gamma=90$, $\beta=91.18$	$2\times3\times3$
Orthorhombic AlH_3 ($P2_1/c$)	$a=13.07$, $b=8.99$, $c=9.43$; $\alpha=\gamma=90$, $\beta=88.09$	$2\times3\times3$
Orthorhombic AlH_3 ($Pbcm$)	$a=8.99$, $b=9.43$, $c=13.06$; $\alpha=\beta=\gamma=90$	$3\times3\times2$
Orthorhombic AlH_3 ($Pnma$)	$a=9.43$, $b=13.14$, $c=9.03$; $\alpha=\beta=\gamma=90$	$3\times2\times3$
Orthorhombic AlH_3 ($P4/n$)	$a=9.51$, $b=9.51$, $c=13.69$; $\alpha=\beta=\gamma=90$	$3\times3\times2$
Hexagonal AlH_3 ($P6/mmm$)	$a=b=13.14$, $c=10.27$; $\alpha=\beta=\gamma=90$	$2\times2\times2$
Tetragonal AlH_3 ($P4/mbm$)	$a=b=10.33$, $c=9.85$; $\alpha=\beta=\gamma=90$	$2\times2\times2$

is calculated by combining calculated and measured data,

$$G_{(p_0=1\ \mathrm{atm},T)}(\mathrm{H_2}) = E_{\mathrm{elec}}(\mathrm{H_2}) + E_{\mathrm{ZP}}(\mathrm{H_2}) + \Delta G_{(T)}(\mathrm{H_2}), \quad (3)$$

where $E_{\mathrm{elec}}(\mathrm{H_2})$ is the electronic energy of a H_2 molecule obtained from the total-energy calculations and $E_{\mathrm{ZP}}(\mathrm{H_2})$ is the zero-point energy of a H_2 molecule obtained from the phonon calculations. $\Delta G_{(T)}(H_2)$ is the temperature-dependent Gibbs free energy with respect to that at 0 K, which can be obtained from the tabulated thermochemical data.[37]

Previous studies of similar hydrides indicate that thermodynamic properties (reaction enthalpy and free energy) are insensitive to the use of the quasiharmonic approximation (QHA) or the harmonic approximation (HA), e.g., for $LiBH_4$ in Ref. 38 and $LiAlH_4$ (Li_3AlH_6 and LiH) in Ref. 39. Usually, the calculated free energy (for both reactant and product) obtained from the QHA is larger than that obtained from the HA. The reaction free energy is calculated by the energy *differences* between the reactant and product, and thus the energy differences are largely canceled out.[39] To make sure that this rule is also applicable for AlH_3, we performed a test for the reaction enthalpy (reaction free energy) of the α-phase AlH_3 and found that the differences obtained using the two approaches are negligible. We will therefore report only the results obtained using the HA in the present paper.

III. RESULTS AND DISCUSSION

To explore the crystal structures of aluminum hydride AlH_3, we have checked a wide variety of AB_3-type candidates. They include LaF_3 [space groups $P\bar{3}c1$,[40] $I4/mmm$,[40] $P6_3/mmc$,[41] and $P6_3cm$ (Ref. 42)], $AsCu_3$ [space groups $I\bar{4}3d$ (Ref. 43) and $P\bar{3}c1$ (Ref. 44)], UO_3 [space groups $I4_1/amd$, $Fddd$,[45] $P21$,[46] $P2_12_12_1$,[47] $Amm2$,[48] and $Pm\bar{3}m$ (Ref. 49)], ReO_3 [space groups $Pm\bar{3}m$,[50] $Pbcn$,[51] $Im\bar{3}$,[52] and $P6_322$ (Ref. 53)], $AlBr_3$ [space group $P2_1/c$ (Ref. 54)], CrO_3 [space group $Ama2$ (Ref. 55)], $FeGe_3$ [space group $Fm\bar{3}m$ (Ref. 56)], AlF_3 (space groups $P4/mbm$ and $P4/nmm$),[57] MoO_3 [space group $Pnma$ (Ref. 58)], and WO_3 [space groups $P6/mmm$ (Ref. 59) and $P4/ncc$ (Ref. 60)], and AB_3 (A=Al, Fe, Ce, Co, Mn, and U; B=F, Cl, etc.). For each structure, the cell volume, shape, and the atom coordinates are fully optimized until the forces are less than 0.0002 eV/Å per atom. After the systematic calculations, six different low-energy structures have been identified. The space groups for these structures are $Pnma$, $P6/mmm$, $I4/mcm$, $P4/mbm$, $P4/nmm$, and $Pm\bar{3}m$, respectively. Their geometric structures are presented in Fig. 1, and their lattice constants and atomic coordinates are compiled in Table II.

The total energies with and without including ZP energies for these structures are calculated and compiled in Table III. For comparison, the energies for α- and γ-AlH_3 are calculated and also listed in the same table. Overall, the total energies and the ZP energies for these structures are close to each other. It is noted that the E_{ZP} for AlH_3 with space groups $Pm\bar{3}m$, $P6/mmm$, $I4/mcm$, $P4/mbm$, and $P4/nmm$ were not calculated because of unstable modes (as discussed in Sec. IV). Results in Table III show that the energy for the AlH_3 ($Pnma$) is close to that for γ-AlH_3. The total energies for the AlH_3 ($P6/mmm$) are very close to that for α-AlH_3. The results that the energies for these different structures are

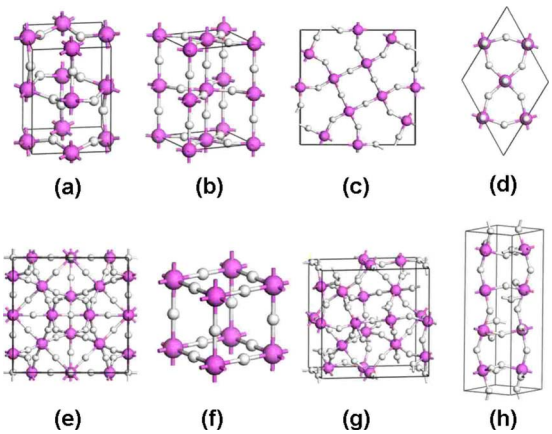

FIG. 1. (Color online) Crystal structures for aluminum hydride AlH_3 with space groups (a) $Pnma$, (b) $I4/mcm$, (c) $P4/mbm$, (d) $P6/mmm$, (e) $P4/nmm$, (f) $Pm\bar{3}m$, (g) $P4/n$, and (h) $Pbcm$. Big and small balls represent Al and H atoms, respectively.

TABLE II. Calculated lattice constants and fractional coordinates for six different structures. The prototypes for cubic ($Pm\bar{3}m$), hexagonal ($P6/mmm$), orthorhombic ($Pnma$), and tetragonal ($I4/mcm$, $P4/mbm$, and P_4/nmm) are ReO_3 ($Pm\bar{3}m$), WO_3 ($P6/mmm$), MoO_3 ($Pnma$), WO_3 ($P4/ncc$), AlF_3 ($P4/mbm$), and AlF_3 ($P4/nmm$), respectively.

Structures	Lattice constants	Atomic coordinates
Cubic ($Pm\bar{3}m$)	a=3.4161 Å	H(0.5,0,0); Al(0,0,0)
Hexagonal ($P6/mmm$)	$a=b=6.568$ Å, $c=3.422$ Å, $\alpha=\beta=90°$, $\gamma=120°$	H1(0.413,0.207,0.5); H2(0.5,0,0); Al(0.5,0,0.5)
Orthorhombic ($Pnma$)	$a=4.713$ Å, $b=6.569$ Å, $c=4.514$ Å, $\alpha=\beta=\gamma=90°$	H1(0.807,0.944,0.188); H2(0.976,0.75,0.612); Al(0.5,0.5,0)
Tetragonal ($I4/mcm$)	$a=b=4.716$ Å, $c=6.844$ Å, $\alpha=\beta=\gamma=90°$	H1(0.691,0.809,0.5); H2(0.5,0.5,0.25); Al(0.5,0.5,0)
Tetragonal ($P4/mbm$)	$a=b=10.883$ Å, $c=3.421$ Å, $\alpha=\beta=\gamma=90°$	H1(0.358,0.432,0); H2(0.505,0.156,0); H3(0.424,0.290,0.5); H4(0.218,0.718,0); H5(0,0.5,0.5); Al1(0.425,0.291,0); Al2(0,0.5,0)
Tetragonal (P_4/nmm)	$a=b=9.632$ Å, $c=6.841$ Å, $\alpha=\beta=\gamma=90°$	H1(0.872,0.805,0.836); H2(0.5,0.825,0.421); H3(0.5,0,0.661); H4(0.5,0,0.159); H5(0.371,0.871,0.905); H6(0.372,0.628,0.5); H7(0,0,0.238); Al1(0.25,0.75,0); Al2(0.5,0.662,0.332); Al3(0.5,0,0.410); Al4(0.5,0,0.909)

very close to the existing α- or γ-AlH_3 indicate that they may exist in the real material. It is noted that mechanical stability of these structures cannot be judged from the total energy alone since they could show dynamic instabilities. To this end, we have performed calculations within the harmonic approximation to determine the phonon-dispersion curves and phonon density of states for these six different structures. The phonon-dispersion curves in Figs. 2(b)–2(f) show that unstable modes exist in AlH_3 with space groups $P6/mmm$, $I4/mcm$, $P4/mbm$, $P4/nmm$, and $Pm\bar{3}m$, indicating that these structures are mechanically unstable. Meanwhile, no unstable mode is obtained for the orthorhombic AlH_3 ($Pnma$), suggesting that synthesis of this structure is feasible.

Concerning the unstable modes for the identified $Pm\bar{3}m$, $I4/mcm$, $P6/mmm$, $P4/mbm$, and $P4/nmm$ structures, it is interesting to search their alternative stable structures along the negative frequencies by applying *ab initio* MD technique. To do that, we applied the procedure similar to Siegel *et al.* in Ref. 61. The enlarged supercells and applied temperature in our MD simulations are compiled in Table IV. At ~2 ps intervals the possible different structures generated from MD simulations are stored, and then these candidates are fully optimized including volume, shape, and atomic coordinates until the Hellmann-Feynman forces are less than 0.0002 eV/Å/atom. The symmetry was determined after the optimization, and as a result four different structures were identified. The space groups for the four structures are $Pbcm$, $P2_1/m$,

TABLE III. Calculated total-energy (E_{tot}) and zero-point energy (E_{ZP}) for ten different structures. Space groups for these structures are $Pnma$, $P6/mmm$, $I4/mcm$, $P4/mbm$, and $P4/nmm$. For contrast, the energies for α- and γ-AlH_3 are also presented in this table. The ΔE is the energy ($E_{tot}+E_{ZP}$) for these structures with respect to the α-AlH_3. Note that the E_{ZP} for space groups $Pm\bar{3}m$, $P2_1/m$, $P2_1/c$, $P6/mmm$, $I4/mcm$, $P4/mbm$, and $P4/nmm$ were not calculated because of unstable modes. Space groups $P2_1/m$, $Pbcm$, and $P4/n$ were obtained from searches along negative frequencies of $Pm\bar{3}m$ (or $I4/mcm$), $I4/mcm$, and $P4/nmm$, respectively.

Structures	Space group	E_{tot} (eV/f.u.)	E_{ZP} (meV/f.u.)	$E_{tot}+E_{ZP}$ (eV/f.u.)	ΔE (meV/f.u.)
α phase	$R\bar{3}c$	−14.056	660	−13.396	0
γ phase	$Pnnm$	−14.033	659	−13.374	22
Orthorhombic	$Pnma$	−14.048	665	−13.383	13
Orthorhombic	$Pbcm$	−14.052	663	−13.389	7
Tetragonal	$P4/n$	−14.022	647	−13.375	21
Cubic	$Pm\bar{3}m$	−13.992			
Orthorhombic	$P2_1/m$	−14.032			
Orthorhombic	$P2_1/c$	−14.052			
Hexagonal	$P6/mmm$	−14.054			
Tetragonal	$I4/mcm$	−14.012			
Tetragonal	$P4/mbm$	−14.029			
Tetragonal	$P4/nmm$	−14.018			

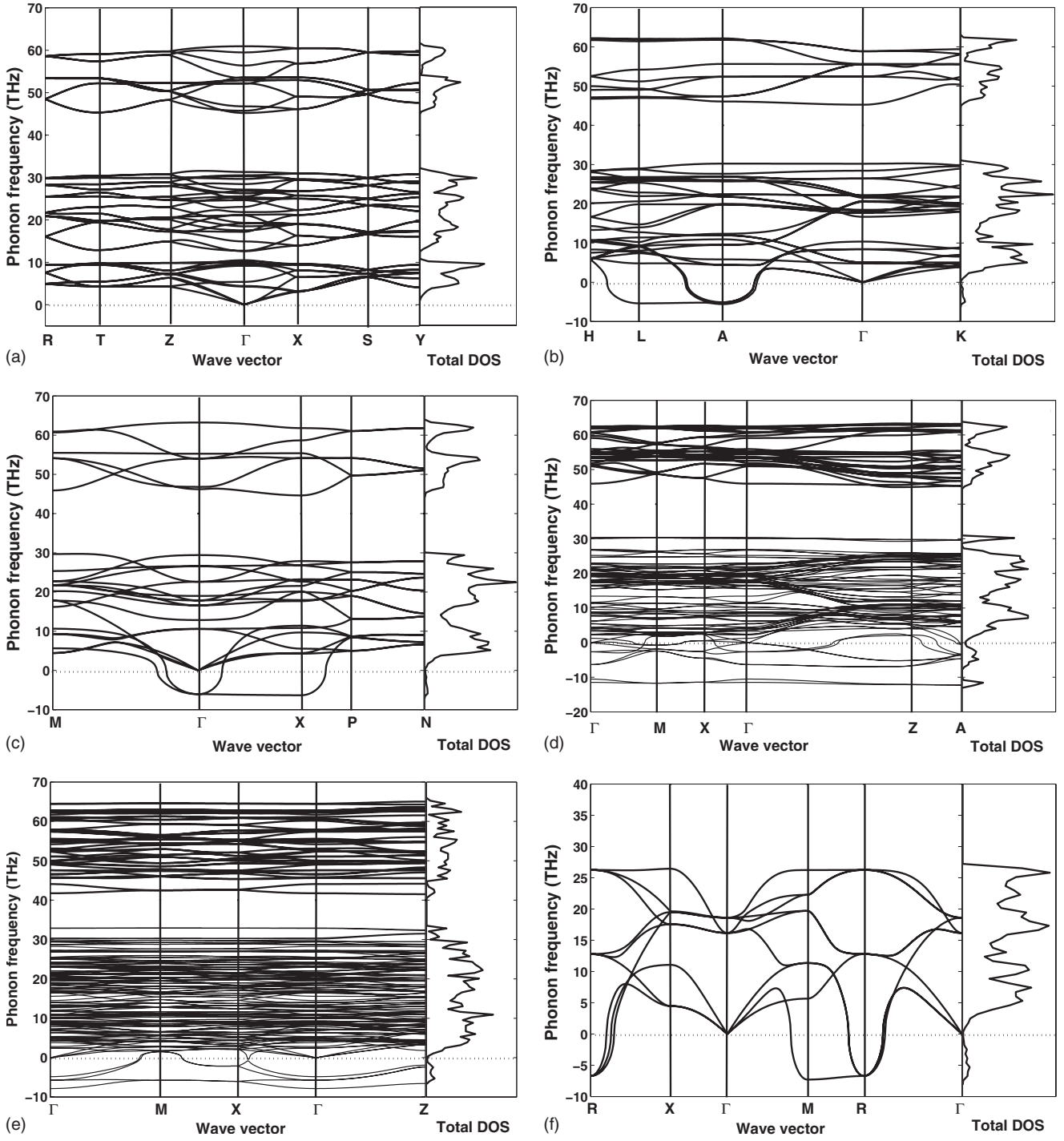

FIG. 2. Calculated phonon-dispersion curves and phonon DOS for the six predicted structures of AlH_3. Panels (a), (b), (c), (d), (e), and (f) represent the phonons for AlH_3 with space groups *Pnma*, *P*6/*mmm*, *I*4/*mcm*, *P*4/*mbm*, *P*4/*nmm*, and $Pm\bar{3}m$, respectively. In each panel, the phonon dispersion relation is presented on the left side and the phonon DOS is shown on the right side.

$P2_1/c$, and $P4/n$. The lattice constants and atomic coordinates for these structures are compiled in Table V, and the total energies are shown in Table III. Energetically, Table III shows that these structures were found to be 4–40 meV/f.u. lower than the original structures. Concerning AlH_3 with space groups *P*6/*mmm* and *P*4/*mbm*, Table IV demonstrates that no alternative structure was found from the MD simulations (even larger supercells were used). The reason is unknown. Probably, the supercell sizes we used are still not big enough. But a large supercell (e.g., 960 atoms, double supercell of *P*4/*mbm*) for 30 ps MD simulations is beyond our computational capability.

To check the mechanical stability for these different crystals (*Pbcm*, $P2_1/m$, $P2_1/c$, and $P4/n$), the phonons were calculated based on the harmonic approximation. The calculations show that AlH_3 with space groups of $P2_1/m$ and

TABLE IV. Supercell size and applied temperature in *ab initio* MD for AlH_3 with space groups $Pm\bar{3}m$, $I4/mcm$, $P6/mmm$, $P4/mbm$, and $P4/nmm$. The simulations were performed on the basis of canonical ensemble by using the algorithm of Nose at temperature 500 K, and typical time step was set to 2 fs. The last column contains different structures obtained from the MD simulations and structural optimization.

Original structures	Temperature (K)	Time (ps)	Supercell size (Å × Å × Å)	Total atoms	Different structures
Cubic cell ($Pm\bar{3}m$)	500	30	13.7 × 13.7 × 13.7	256	Orthorhombic ($P2_1/m$)
Tetragonal	500	10	9.4 × 9.4 × 13.7	128	Orthorhombic ($P2_1/m$)
($I4/mcm$)	500	16	9.4 × 9.4 × 13.7	128	Orthorhombic ($P2_1/c$)
	500	30	9.4 × 9.4 × 13.7	128	Orthorhombic ($Pbcm$)
Hexagonal	500	30	13.1 × 11.4 × 10.3	144	Unchanged
($P6/mmm$)	500	15	19.7 × 11.4 × 10.3	216	Unchanged
Tetragonal	500	30	10.9 × 10.9 × 10.3	120	Unchanged
($P4/mbm$)	500	15	20.7 × 20.7 × 9.8	480	Unchanged
Tetragonal ($P4/nmm$)	500	30	9.6 × 9.6 × 13.7	128	Tetragonal ($P4/n$)

$P2_1/c$ have unstable modes (not plotted here), indicating that they are mechanically unstable. This may be understood from the process of the MD simulations, e.g., Table IV shows that these two structures appear at 10–16 ps from the original AlH_3 ($I4/mcm$) at 500 K, and then they disappear one after the other at ~30 ps, indicating that the two structures may be intermediate states. The phonon-dispersion curves for the $Pbcm$ and $P4/n$ are presented in Figs. 3(a) and 3(b), respectively. It can be seen from the figures that no unstable mode is observed for these two structures, suggesting that the synthesis of the two structures may be feasible.

Because of unstable modes, thermodynamic functions for AlH_3 with space groups $Pm\bar{3}m$, $P6/mmm$, $I4/mcm$, $P4/mbm$, $P4/nmm$, $P2_1/c$, and $P2_1/m$ cannot be accurately

TABLE V. Calculated lattice constants and fractional coordinates for four different structures which are obtained from *ab initio* molecular dynamics.

Structures	Lattice constants	Atomic coordinates
Orthorhombic ($Pbcm$)	a=4.499 Å, b=4.714 Å, c=13.063 Å $\alpha=\beta=\gamma=90°$	H1(0.4390.533,0.846); H2(0.063,0.919,0.5949); H3(0.631,0.75,0.5); H4(0.132,0.203,0.75); Al(0.75,0.727,0.875).
Tetragonal ($P4/n$)	$a=b$=9.509 Å, c=6.847 Å $\alpha=\beta=\gamma=90°$	H1(0.86,0.174,0.658); H2(0.617,0.715,0.331); H3(0.951,0.328,0.914); H4(0.887,0.354,0.405); H5(0.885,0.855,0.007); H6(0.5,0.5,0.257); H7(0,0.5,0.158); H8(0,0.5,0.658); Al1(0.512,0.336,0.168); Al2(0.5,0,0.093); Al3(0.5,0,0.592); Al4(0.75,0.25,0.5)
Monoclinic ($P2_1/m$)	a=13.118 Å, b=6.581 Å, c=6.544 Å; $\alpha=\gamma=90°$, β=91.18°	H1(0.779,0.055,0.761); H2(0.278,0.055,0.741); H3(0.528,0.946,0.251); H4(0.029,0.055,0.251); H5(0.375,0.048,0.430); H6(0.874,0.053,0.447); H7(0.374,0.556,0.041); H8(0.877,0.556,0.063); H9(0.529,0.25,0.457); H10(0.021,0.25,0.566); H11(0.782,0.75,0.555); H12(0.28,0.75,0.533); H13(0.523,0.75,0.937); H14(0.034,0.75,0.042); H15(0.773,0.25,0.076); H16(0.271,0.25,0.054); Al1(0.75,0,0.51); Al2(0.751,0.5,0.01); Al3(0.5,0,0); Al4(0,0,0); Al5(0.5,0.5,0.5); Al6(0,0.5,0.5).
Monoclinic ($P2_1/c$)	a=13.064 Å, b=4.497 Å c=4.713 Å; $\alpha=\gamma=90°$, β=88.07°	H1(0.971,0.187,0.695); H2(0.470,0.312,0.809); H3(0.719,0.813,0.334); H4(0.222,0.812,0.285); H5(0.624,0.121,0.012); H6(0.126,0.116,0.964) Al1(0.749,0,0.024); Al2(0,0,0); Al3(0.5,0,0).

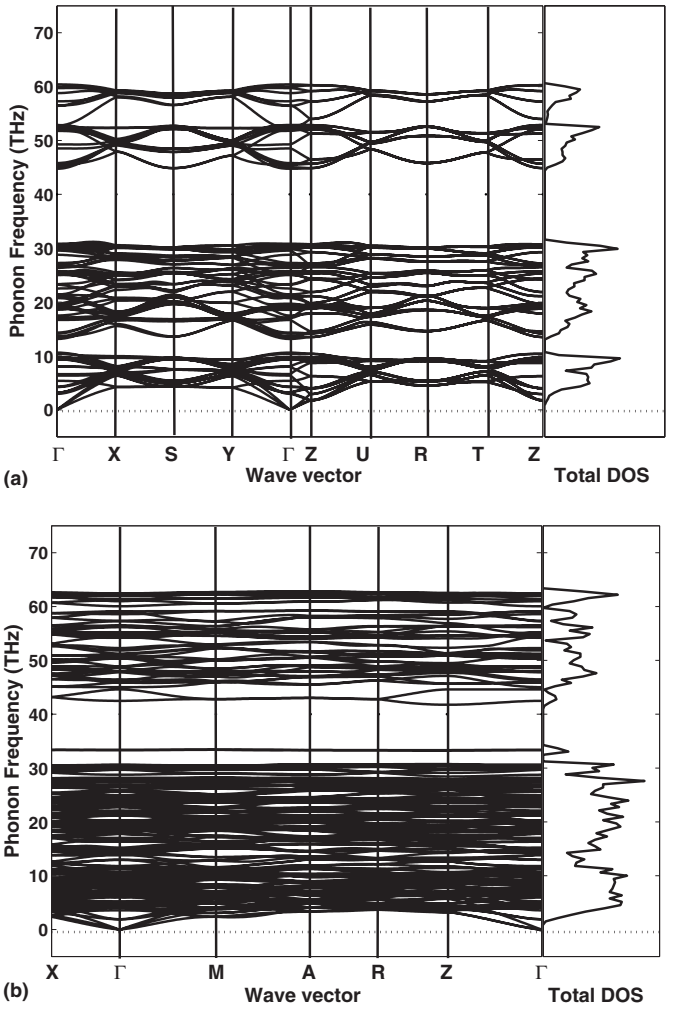

FIG. 3. Calculated phonon-dispersion curves and phonon DOS for AlH_3 with space groups (a) *Pbcm* and (b) $P4/n$.

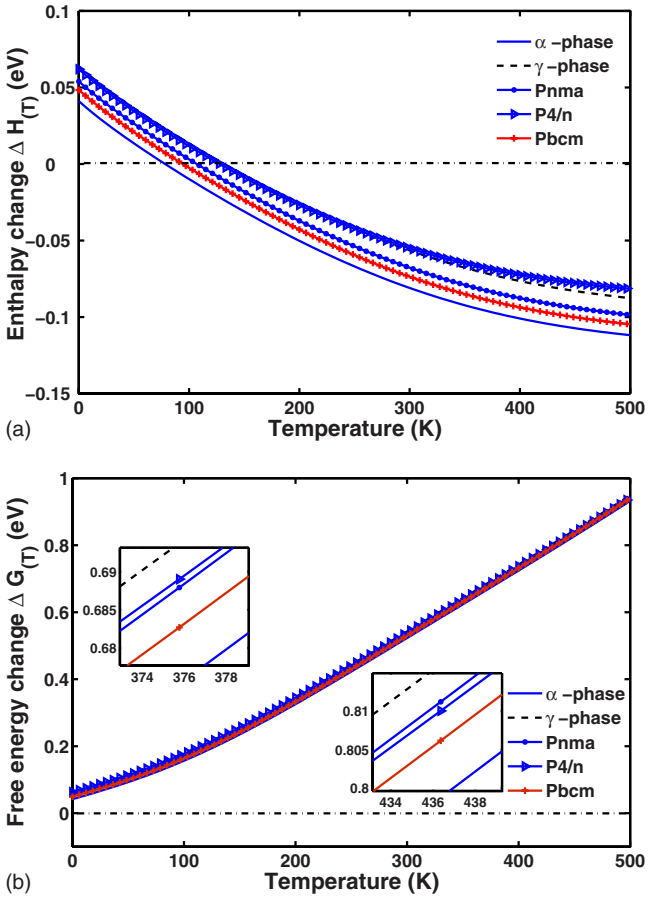

FIG. 4. (Color online) Calculated (a) enthalpy changes and (b) Gibbs free-energy changes for Eq. (1) as a function of temperature at atmospheric pressure. Solid line, dashed line, solid line with ●, solid line with ▶, and solid line with + represent the data for α-, γ-, orthorhombic (*Pnma*), tetragonal ($P4/n$), and orthorhombic (*Pbcm*) AlH_3, respectively.

determined from the integral of phonon DOS, and thus their thermodynamic stabilities are not discussed in the current study. Nevertheless, as pointed out in a recent work,[62] unstable modes may be permitted in one component of a composite material when the overall stability of the composite material is still maintained. This scenario may help stabilize these AlH_3 phases that are unstable in their pure phases at low temperatures. We carried out an analysis of the thermodynamic stability of the three different AlH_3 phases (*Pnma*, *Pbcm*, and $P4/n$) by calculating the reaction enthalpy and reaction Gibbs free energy. The reaction enthalpy (or reaction Gibbs free energy) is calculated by the energy difference between the reactant and product in Eq. (1) (reactant *minus* product). A positive Gibbs free-energy change means that the product is more stable than the reactant, and a negative enthalpy change means that the reaction is endothermic. Figure 4 shows the calculated reaction enthalpy and reaction Gibbs free-energy changes as a function of temperature at atmospheric pressure. For comparison, the calculated energies for α- and γ-AlH_3 are also shown in Fig. 4. The results show that both the reaction enthalpy and free energy for the three different crystals are close to the existing α- and γ-AlH_3, in which the orthorhombic AlH_3 (*Pbcm*) is closer to the α-AlH_3 and the tetragonal AlH_3 ($P4/n$) is closer to the γ-AlH_3. Overall, the thermodynamic properties among these structures are similar; thus the conclusions are similar to those drawn for the α-AlH_3 by Wolverton *et al.*,[2] i.e., the enthalpy changes indicate that the reactions are endothermic, and the free-energy changes indicate that the decompositions may take place spontaneously.

Finally, we present simulated x-ray powder-diffraction patterns for several different structures of AlH_3 that may offer further insights into the structural characterization of these different phases. Comparing results in Fig. 5(a) with those in Figs. 5(b) and 5(c), one can see that they are very similar (there are some differences in peaks at $2\theta = \sim 40°$), indicating that the orthorhombic AlH_3 (*Pbcm* and *Pnma*) could be easily identified by mistake as the α-AlH_3 in structural refinements. It can be seen from the figure that the main-peak positions for the simulated AlH_3 ($P4/n$) are in good agreement with the experimental δ-AlH_3, indicating that the space group for the δ-AlH_3 may be $P4/n$. For the tetragonal AlH_3 ($P4/mbm$), its pattern partially agrees with the experimental data at some peaks. These results show that careful analysis and further structural characterization are needed to distinguish these different AlH_3 phases that exhibit

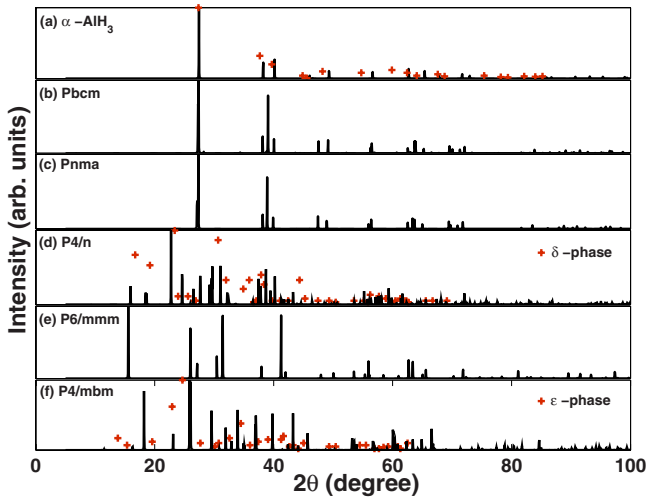

FIG. 5. (Color online) Simulated x-ray powder-diffraction patterns for six different AlH_3. Solid lines in Figs. 4(b)–4(f) represent simulated patterns for AlH_3 with space groups *Pbcm*, *Pnma*, *P*4/*n*, *P*6/*mmm*, and *P*4/*mbm*, respectively. The experimental data from Ref. 24 are denoted as red +. For comparison, calculated and experimental patterns for α-AlH_3 are shown in Fig. 5(a).

different atomic bonding environments but share considerable similarities in x-ray diffraction patterns.

Since the above x-ray patterns among AlH_3 with space groups $R\bar{3}c$, *Pbcm*, and *Pnma* are quite similar, it is necessary to further investigate these patterns by using a full Rietveld refinement method. The advantage of Rietveld refinement over the usual method is the use of full-pattern fitting, e.g., all lines for each phase are explicitly taken into account and even overlapped lines are also not problematic, which is a major problem with the usual fitting method.[63,64]

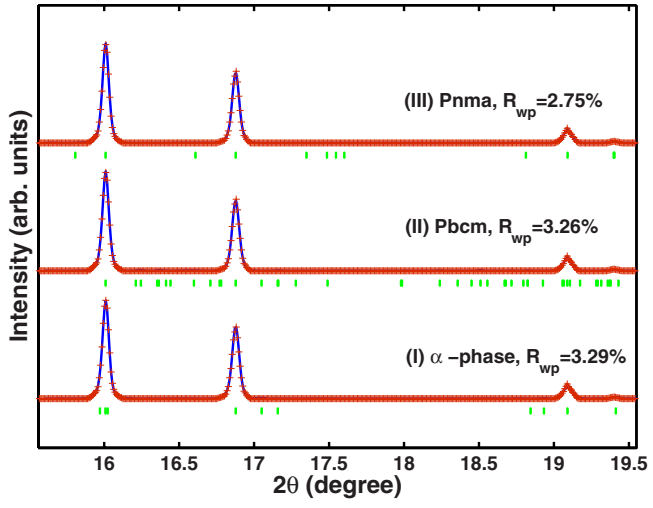

FIG. 6. (Color online) X-ray powder-diffraction patterns for AlH_3 with Rietveld profile fits (solid lines) using space groups (I) $R\bar{3}c$, (II) *Pbcm*, and (III) *Pnma*. Experimental data are denoted as +, in which x-ray wavelength of $\lambda = 0.6541$ Å was used. Experimental data were taken point by point from Ref. 13 by using the WINFIG software (Ref. 65). The short green bars (bottom) are observed reflections for simulated patterns.

Figure 6 shows the simulated x-ray powder-diffraction patterns for AlH_3 with Rietveld profile fits by using space groups $R\bar{3}c$, *Pbcm*, and *Pnma*. The experimental data for α-AlH_3 are from Ref. 13, in which Lebail profile fits[66,67] were performed by Graetz *et al.*[13] The value of R_{wp} is used to measure the similarity between the simulated and experimental diffraction patterns. The smaller the value, the better the agreement. It is shown from Fig. 6 that the R_{wp} for the $R\bar{3}c$, *Pbcm*, and *Pnma* are 3.29%, 3.26%, and 2.75%, respectively. These values are close to each other, indicating that fitting these space groups to the experimental α-AlH_3 data gives almost the same satisfactory result. This is an interesting result. The result indicates that the space group for the α-AlH_3 phase cannot be judged from Rietveld refinement. According to the energetic ordering of free energy in Fig. 4, the AlH_3 ($R\bar{3}c$) is more stable than the AlH_3 (*Pbcm*), which in turn is more stable than the AlH_3 (*Pnma*). Thus the AlH_3 ($R\bar{3}c$) is the most stable among the three phases, indicating that the space group for the α-AlH_3 phase is likely $R\bar{3}c$. It is noted that the stability of a material also depends on reaction kinetics, but the kinetics cannot be judged from these free energies.

Since the x-ray diffraction patterns for the orthorhombic AlH_3 (*Pbcm* and *Pnma*) is quite similar to the α-AlH_3 ($R\bar{3}c$), one may suspect that these two different structures may become α-AlH_3 ($R\bar{3}c$) if one determines their symmetries by using different tolerances. To check this, the space groups for the two structures were carefully determined by using different criteria (tolerance range from 0.0001 to 0.5 Å), and the results found that these two symmetries always remain un-

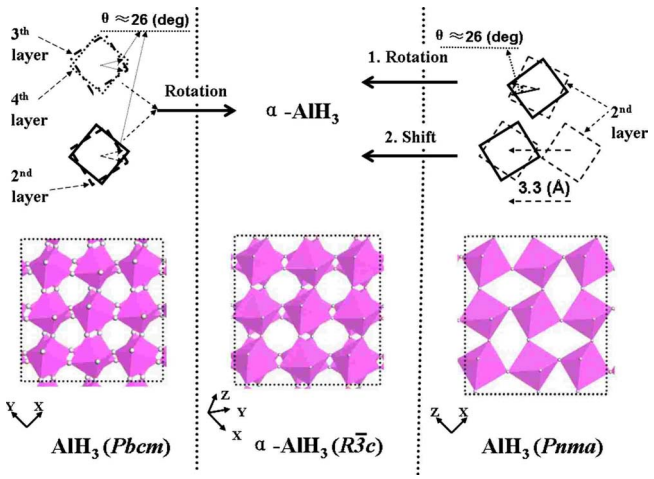

FIG. 7. (Color online) Structural comparison among AlH_3 with space groups $R\bar{3}c$ (middle), *Pbcm* (left side), and *Pnma* (right side). On top-right (and left) side, solid and dashed squares represent octahedra in the first and second layers, respectively. On top-left side, dashed-dotted and dotted squares represent the octahedra in the third and fourth layers, respectively. The crystal stacking planes for α-AlH_3 ($R\bar{3}c$) and AlH_3 (*Pnma*) are in *ABA* arrangements, but for AlH_3 (*Pnma*) the second layer is invisible since it overlaps with the first layer. The stacking planes for AlH_3 (*Pbcm*) is in *ABCD* arrangement (it is noted that the third and fourth layers are invisible since they overlap with the second and first layers, respectively).

changed. To check geometrical differences, a structural comparison among the three phases ($R\bar{3}c$, *Pbcm*, and *Pnma*) is shown in Fig. 7. It can be seen from the figure that the orientations of octahedra among the three phases are different to some extent. Roughly, α-AlH_3 ($R\bar{3}c$) can be obtained from the AlH_3 (*Pnma*) through the following two ways, i.e., either all octahedra in the second layer rotate at an angle of ~26° or the octahedra shift at a distance of ~3.3 Å (see the top-right side of Fig. 7). Alternatively, α-AlH_3 ($R\bar{3}c$) can be obtained from another AlH_3 (*Pbcm*) through rotating the octahedra in the second and fourth layers by ~26° (see the top-left side of Fig. 7).

IV. SUMMARY

In summary, we have identified ten different low-energy structures for aluminum hydride AlH_3 from first-principles calculations. Energetically, these structures are close to the existing α- and γ-AlH_3. The space groups for these structures are *Pnma*, $P6/mmm$, $I4/mcm$, $P4/mbm$, $P4/nmm$, $Pm\bar{3}m$, $P2_1/m$, $P2_1/c$, *Pbcm*, and $P4/n$. The calculated phonon-dispersion curves reveal unstable modes in structures with space groups $P6/mmm$, $I4/mcm$, $P4/mbm$, $P4/nmm$, $Pm\bar{3}m$, $P2_1/m$, and $P2_1/c$, indicating that these seven structures are unstable at low temperatures. Still, they may exist as minority phases in real samples at appropriate temperatures. Meanwhile, no unstable modes were found in the AlH_3 with space groups *Pnma*, *Pbcm*, and $P4/n$. Overall, the calculated results show that both the reaction enthalpy and free energy for the three different crystals are close to the existing α- and γ-AlH_3. According to x-ray powder-diffraction patterns, the simulated main-peak positions for the AlH_3 ($P4/n$) are in good agreement with the experimental δ-AlH_3. A full Rietveld analysis reveals that fitting the space groups $R\bar{3}c$, *Pbcm*, and *Pnma* to the experimental x-ray powder-diffraction pattern of α-AlH_3 gives almost the same satisfactory result.

ACKNOWLEDGMENTS

We thank O. M. Løvvik, Z. Y. Zhu, and J. J. Zhao for useful discussion. Financial support from NSF of China with Grants No. 10504007 and No. 10635040, SRF for ROCS, State Education Ministry, and Shanghai supercomputer center are acknowledged. Work at UNLV was supported by the U.S. Department of Energy under Grants No. DE-FG36-05GO085028 and No. DE-FC52-06NA26274.

*xzke@phy.ecnu.edu.cn
†chen@physics.unlv.edu
‡isao.tanaka@materials.mbox.media.kyoto-u.ac.jp

[1] A. Aguayo and D. J. Singh, Phys. Rev. B **69**, 155103 (2004).
[2] C. Wolverton, V. Ozoliņš, and M. Asta, Phys. Rev. B **69**, 144109 (2004).
[3] X. Ke, A. Kuwabara, and I. Tanaka, Phys. Rev. B **71**, 184107 (2005).
[4] C. J. Pickard and R. J. Needs, Phys. Rev. B **76**, 144114 (2007).
[5] M. J. van Setten, V. A. Popa, G. A. de Wijs, and G. Brocks, Phys. Rev. B **75**, 035204 (2007).
[6] A. Goldberg and I. Yarovsky, Phys. Rev. B **75**, 195403 (2007).
[7] S. Sartori, S. M. Opalka, O. M. Løvvik, M. N. Guzik, X. Tang, and B. C. Hauback, J. Mater. Chem. **18**, 2361 (2008).
[8] Y. Wang, J. A. Yan, and M. Y. Chou, Phys. Rev. B **77**, 014101 (2008).
[9] S. Z. Karazhanov, A. G. Ulyashin, P. Ravindran, and P. Vajeeston, Europhys. Lett. **82**, 17006 (2008).
[10] C. Wolverton, D. J. Siegel, A. R. Akbarzadeh, and V. Ozoliņš, J. Phys.: Condens. Matter **20**, 064228 (2008).
[11] R. H. Scheicher, D. Y. Kim, S. Lebegue, B. Arnaud, M. Alouani, and R. Ahuja, Appl. Phys. Lett. **92**, 201903 (2008).
[12] H. W. Brinks, A. Istad-Lem, and B. C. Hauback, J. Phys. Chem. B **110**, 25833 (2006).
[13] J. Graetz, S. Chaudhuri, Y. Lee, T. Vogt, J. T. Muckerman, and J. J. Reilly, Phys. Rev. B **74**, 214114 (2006).
[14] G. Sandrock, J. Reilly, J. Graetz, W. M. Zhou, J. Johnson, and J. Wegrzyn, J. Alloys Compd. **421**, 185 (2006).
[15] J. Graetz and J. J. Reilly, J. Alloys Compd. **424**, 262 (2006).
[16] S. Orimo, Y. Nakamori, T. Kato, C. Brown, and C. M. Jensen, Appl. Phys. A: Mater. Sci. Process. **83**, 5 (2006).
[17] H. W. Brinks, W. Langley, C. M. Jensen, J. Graetz, J. J. Reilly, and B. C. Hauback, J. Alloys Compd. **433**, 180 (2007).
[18] V. A. Yartys, R. V. Denys, J. P. Maehlen, C. Frommen, M. Fichtner, B. M. Bulychev, and H. Emerich, Inorg. Chem. **46**, 1051 (2007).
[19] H. W. Brinks, C. Browns, C. M. Jensen, J. Graetz, J. J. Reilly, and B. C. Hauback, J. Alloys Compd. **441**, 364 (2007).
[20] A. I. Kolesnikov, V. E. Antonov, Y. E. Markushkin, I. Natkaniec, and M. K. Sakharov, Phys. Rev. B **76**, 064302 (2007).
[21] H. Grove, M. H. Sørby, H. W. Brinks, and B. C. Hauback, J. Phys. Chem. C **111**, 16693 (2007).
[22] I. Goncharenko, M. I. Eremets, M. Hanfland, J. S. Tse, M. Amboage, Y. Yao, and I. A. Trojan, Phys. Rev. Lett. **100**, 045504 (2008).
[23] *Hydrogen in Metals II*, edited by G. Alefeld and J. Völkl, Topics in Applied Physics Vol. 29 (Springer, Berlin, 1978).
[24] F. M. Brower, N. E. Matzek, P. F. Reigler, H. W. Rinn, C. B. Roberts, D. L. Schmidt, J. A. Snover, and K. Terada, J. Am. Chem. Soc. **98**, 2450 (1976).
[25] J. W. Turley and H. W. Rinn, Inorg. Chem. **8**, 18 (1969).
[26] W. Kohn and L. J. Sham, Phys. Rev. **140**, A1133 (1965).
[27] P. Hohenberg and W. Kohn, Phys. Rev. **136**, B864 (1964).
[28] J. P. Perdew, J. A. Chevary, S. H. Vosko, K. A. Jackson, M. R. Pederson, D. J. Singh, and C. Fiolhais, Phys. Rev. B **46**, 6671 (1992).
[29] G. Kresse and J. Furthmüller, Comput. Mater. Sci. **6**, 15 (1996).
[30] G. Kresse and J. Furthmüller, Phys. Rev. B **54**, 11169 (1996).
[31] P. E. Blöchl, Phys. Rev. B **50**, 17953 (1994).
[32] G. Kresse and D. Joubert, Phys. Rev. B **59**, 1758 (1999).
[33] H. J. Monkhorst and J. D. Pack, Phys. Rev. B **13**, 5188 (1976).
[34] K. Parlinski, Z. Q. Li, and Y. Kawazoe, Phys. Rev. Lett. **78**,

4063 (1997).
[35] K. Parlinski, Software PHONON, Institute of Nuclear Physics, Crakow, 2005.
[36] A. A. Maradudin, E. W. Montroll, G. H. Weiss, and I. P. Ipatova, *Theory of Lattice Dynamics in the Harmonic Approximation in Solid State Physics Supplement* (Academic, New York, 1971), Vol. 3.
[37] D. R. Stull and H. Prophet, *JANAF Thermodynamical Tables*, 2nd ed. (U.S. National Bureau of Standards, Washington, DC, 1971).
[38] T. J. Frankcombe and G.-J. Kroes, Phys. Rev. B **73**, 174302 (2006).
[39] X. Ke and C. F. Chen, Phys. Rev. B **76**, 024112 (2007).
[40] B. Winkler, K. Knorr, and V. Milman, J. Alloys Compd. **349**, 111 (2003).
[41] K. Schlyter, Ark. Kemi **5**, 73 (1952).
[42] D. Gregson, C. R. A. Catlow, A. V. Chadwick, G. H. Lander, A. N. Cormack, and B. E. F. Fender, Acta Crystallogr., Sect. B: Struct. Sci. **39**, 687 (1983).
[43] J. E. Iglesias and W. Nowacki, Z. Kristallogr. **145**, 334 (1977).
[44] B. Steenberg, Ark. Kemi, Mineral. Geol., A **12**(2), 1 (1938).
[45] B. O. Loopstra, J. C. Taylor, and A. B. Waugh, J. Solid State Chem. **20**, 9 (1977).
[46] P. C. Debets, Acta Crystallogr. **21**, 589 (1966).
[47] S. Siegel, H. R. Hoekstra, and E. Sherry, Acta Crystallogr. **20**, 292 (1966).
[48] B. O. Loopstra and E. H. P. Cordfunke, Recl. Trav. Chim. Pays-Bas **85**, 135 (1966).
[49] R. J. Ackermann, A. T. Chang, and C. A. Sorrell, J. Inorg. Nucl. Chem. **39**, 75 (1977).
[50] K. Meisel, Z. Anorg. Allg. Chem. **207**, 121 (1932).
[51] A. Magneli, Acta Chem. Scand. (1947-1973) **11**, 28 (1957).
[52] J.-E. Jørgensen, J. D. Jorgensen, B. Batlogg, J. P. Remeika, and J. D. Axe, Phys. Rev. B **33**, 4793 (1986).
[53] T. I. Dyuzheva, N. A. Bendeliani, and S. S. Kabalkina, J. Less-Common Met. **133**, 313 (1987).
[54] S. I. Troyanov, Zh. Neorg. Khim. **39**, 552 (1994).
[55] J. S. Stephens and D. W. J. Cruickshank, Acta Crystallogr., Sect. B: Struct. Crystallogr. Cryst. Chem. **26**, 222 (1970).
[56] R. Sobczak, Monatsch. Chem. **106**, 1389 (1975).
[57] N. Herron, D. L. Thorn, R. L. Harlow, G. A. Jones, J. B. Parise, J. A. Fernandez-Baca, and T. Vogt, Chem. Mater. **7**, 75 (1995).
[58] A. Magneli, Acta Chem. Scand. (1947-1973) **2**, 861 (1948).
[59] B. Gerand, G. Novogorocki, J. Guenot, and M. Figlarz, J. Solid State Chem. **29**, 429 (1979).
[60] K. R. Locherer, I. P. Swainson, and E. K. H. Salje, J. Phys.: Condens. Matter **11**, 4143 (1999).
[61] D. J. Siegel, C. Wolverton, and V. Ozoliņš, Phys. Rev. B **75**, 014101 (2007).
[62] W. J. Drugan, Phys. Rev. Lett. **98**, 055502 (2007).
[63] H. M. Rietveld, J. Appl. Crystallogr. **2**, 65 (1969).
[64] Rietveld refinement software can be found at http://www.ing.unitn.it/~maud/.
[65] WINFIG software, http://user.cs.tu-berlin.de/huluvu/WinFIG.htm.
[66] A. C. Larson and R. B. Vondreele, GSAS, General Structure Analysis System, Los Alamos National Laboratory Report No. LAUR 86-745, 1986 (unpublished).
[67] B. H. Toby, J. Appl. Crystallogr. **34**, 210 (2001).